Applied Catalysis A: General 523 (2016) 321–331

Contents lists available at ScienceDirect

Applied Catalysis A: General

journal homepage: www.elsevier.com/locate/apcata

Heterogenized hybrid catalyst of 1-sulfonic acid-3-methyl imidazolium ferric chloride over NaY zeolite for one-pot synthesis of 2-amino-4-arylpyrimidine derivatives: A viable approach

Pinky Gogoi, Arup Kumar Dutta, Susmita Saikia, Ruli Borah*

Department of Chemical Sciences, Tezpur University, Napaam, 784028, Tezpur, Assam, India

ARTICLE INFO

Article history:
Received 12 February 2016
Received in revised form 10 June 2016
Accepted 10 June 2016
Available online 14 June 2016

Keywords:
Heterogenized hybrid catalyst
1-Sulfonic acid-3-methyl imidazolium ferric chloride salt
NaY zeolite
Extra framework aluminium species
Reusable catalyst
2-Amino-4-arylpyrimidine

ABSTRACT

A new hybrid material of NaY zeolite supported 1-sulfonic acid-3-methyl imidazolium ferric chloride [Msim][$FeCl_4$] has been developed by modifying the zeolite surface with six different w/w ratios through wet impregnation method. These composites were fully characterized by Powder XRD, FT-IR, Raman, TGA, SEM, TEM, EDX, BET, ICP-OES and Hammett acid strength measurement methods. The zeolite framework was found to be remaining preserved up to w/w ratio of 0.2 with some portion of extra framework Al species (EFAl) while crystallinity of the composites decreased from lower to higher loading. The overall thermal stability of composite materials increases up to w/w ratio of 0.1 than NaY. The catalytic performance of composite materials were examined for the novel one-pot consecutive formation of Biginelli- 3,4-dihydropyrimidin-2-(1H)-ones to 2-amino-4-arylpyrimidines. The 0.1 ratio composite material showed excellent catalytic activity up to ten consecutive cycles in solvent-free medium under the optimized reaction condition.

1. Introduction

Encapsulation of ionic liquid salt in microporous solids such as zeolite is an attractive technique for heterogenization, since leaching can be controlled when the salt is confined exclusively in the zeolite pores [1–3]. Zeolites are among the most efficient support for ionic liquids owing to their unique properties such as high surface area, well organized pore channels, good thermal stability, environmentally benign nature and high absorption towards organic compounds. Ionic liquid salts are also characterized by their low melting point, non-flammability, relatively low viscosities, high thermal and chemical stability [4]. The presence of acidic or basic character of ionic liquids makes them more suitable for dual role in organic synthesis as catalyst and recyclable solvent [5–8].

The combination of the two aforementioned types of materials (zeolites and ionic liquids) could result in composite materials suitable for various applications such as separation technology, catalysis and fuel cell [2,9–13]. For example, DeCastro et al., developed 1-butyl-3-methyl-imidazolium chloride and $AlCl_3$ immobilized beta type zeolite for the alkylation of aromatic compounds [14]. Valkenberg et al., also presented three different approaches for the preparation of novel catalysts of supported ILs on zeolites and other porous supports for the Friedel–Crafts reaction [15]. Eguizábala et al., utilized ammonium based ionic liquids immobilized in Y and beta type zeolites by solution methods as hydrophilic-conducting fillers for proton exchange membrane fuel cell [16]. The heterogenization process can easily modify the surface of solid support by transferring some properties of IL phase on to the surface for specific use [17,18]. Such acidic or basic hybrid catalysts can be separated from the product by filtration in any suitable solvent. This type of composite material allows us to design solid material possessing uniform and well-dispersed surface topologies with definite properties and controlled chemical reactivity which may act as 'designer surface'. Hybrid zeolite catalysts have advantages compared to the parent ones in terms of their tunable acidity, hydrophilicity or hydrophobicity and thermal stability.

Pyrimidines are integral part of DNA and RNA, and also have diverse biological activities like anticancer, anti-inflammatory, analgesic, anticonvulsant, anthelmintic and anti-allergic agents [19,20]. 2-Aminopyrimidine unit is the structural motif of several bioactive natural products and finds extensive applications as drug like scaffold in medicinal chemistry such as anti-atherosclerotic Aronixil, anti-histaminic Thonzylamine, anti-anxiolytic Buspirone, HMG-CoA reductase inhibitor Rosuvastatin and anti-cancer drug

* Corresponding author.
E-mail address: ruli@tezu.ernet.in (R. Borah).

http://dx.doi.org/10.1016/j.apcata.2016.06.015
0926-860X/

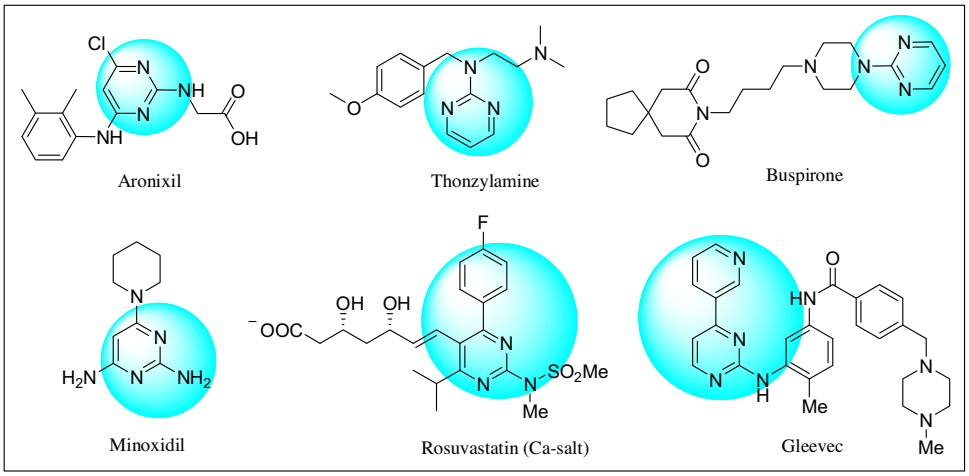

Fig. 1. Commercial drugs with pyrimidine/2-aminopyrimidine/2-amino-4-arylpyrimidine moiety.

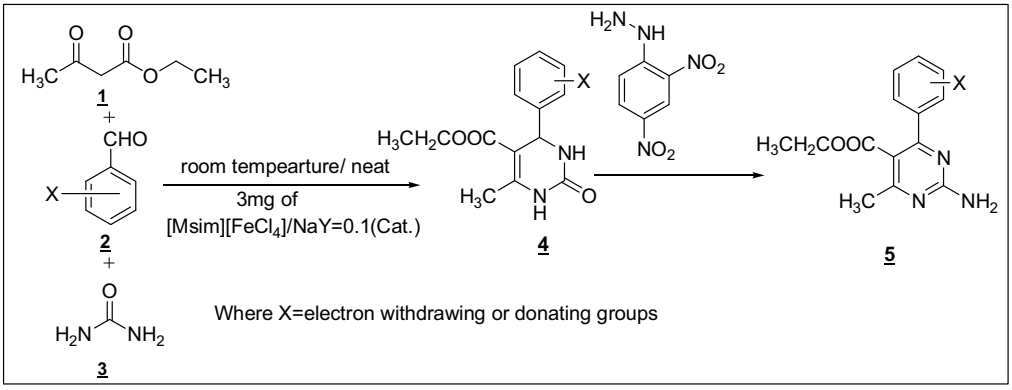

Scheme 1. One pot synthesis of 2-amino-4-arylpyrimidine derivatives via *in situ* formation of DHPMs.

Gleevec (Fig. 1). They are also capable of exhibiting rho-associated protein kinase-1 inhibitor, glycogen synthase kinase-3 inhibitor and N-type calcium channel blockers [21–24]. The Biginelli 3,4-dihydropyrimidinones (DHPMs) are the chemical precursors of multi-functionalized pyrimidines. The preparation of DHPMs involves a three component reaction of β-keto ester, aldehydes and urea (or thiourea) using a variety of acid catalysts at different conditions (Scheme 1) [25–28]. Several modified methods have been developed for the Biginelli reaction till date [29–33]. Despite the connecting link with pyrimidines, there has been lack of efficient methodologies to convert DHPMs to pyrimidines. Few methodologies are available in literature which achieved this by dehydrogenation of the DHPMs followed by nucleophilic substitution at C-2 position [34–36].

Puchala et al., first reported the dehydrogenation of DHPMs by nitric acid with 50–60% of oxidized products [37]. Other methods include the use of ceric ammonium nitrate, (diacetoxyiodo) benzene, $Mn(OAc)_3$ and MnO_2, *tert*-butylhydroperoxide in the oxidative aromatization of 1,4-dihydropyrimidine [38–41]. Quan et al., reported a simple iodine mediated S—N or C—N cross-coupling and oxidative–aromatization of 3,4-dihydropyrimidine-2(1H)-thione with a secondary amine [42]. Kang et al., also synthesized C-2 functionalized pyrimidines via Kappe dehydrogenation of the DHPMs and PyBroP-mediated coupling with nucleophiles at room temperature for 24 h [43]. Most of the known dehydrogenation methods suffer from longer reaction time (36–67 h), higher temperature, and lower yields and inefficiency of the oxidizing agents [34–36]. The inactive nature of DHPMs ring towards various oxidizing agents makes dehydrogenation a more difficult task [36–44]. In 2007, Matoobi et al., introduced a modified sequential five steps microwave assisted conversion of DHPMs to 2-amino-4-aryl pyrimidine derivatives at high temperature in sealed vessel through isolation of each intermediate involved in S-alkylation, oxidation and nucleophilic substitution steps [23].

In this context, there is a scope to develop mild, simpler and more efficient route to construct complex library of pyrimidine derivatives via *in situ* conversion of DHPMs to 2-amino-4-arylpyrimidine derivatives using sequential acid catalyzed condensation-aromatization reactions according to Scheme 1 from the three component Biginelli reactions [45–47].

2. Experimental

2.1. General techniques

All chemicals were purchased from different chemical suppliers and used as received without any further treatment. X-ray diffraction patterns of the prepared samples were recorded using a Rigaku (miniflex UK) X-ray diffractometer with CuKα radiation (0.15418 nm) operated at 30 kV and 15 mA at a scan speed of 2° min^{-1} and 2θ range of 5–70°. The percent crystallinity of the samples was calculated from the XRD peaks by using the formula: %Crystallinity = (Intensity of the characteristic XRD peak of the hybrid catalyst)/(Intensity of the characteristic peak of the base zeolite). The ^{1}HNMR and ^{13}CNMR were recorded on a JEOL 400 MHz spectrometer (δ in ppm) in $CDCl_3$ and DMSO-d_6 solvents. Perkin Elmer FT-IR spectrometer was used to take FT-IR spectra. The Hammett plot of the solid acids was determined on an UV 2550

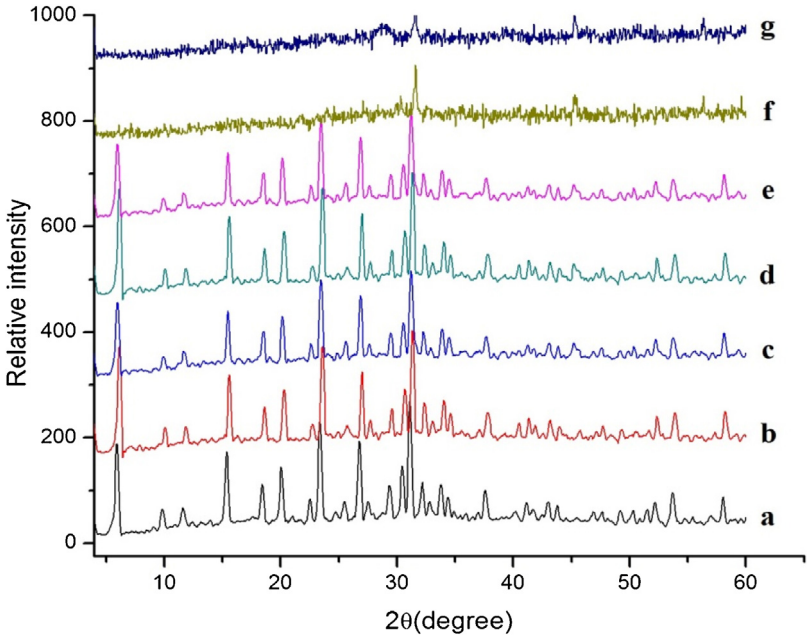

Fig. 2. Powder XRD spectrum of the parent and modified NaY zeolite sample; (a) NaY, (b) [Msim][$FeCl_4$]/NaY = 0.03, (c) [Msim][$FeCl_4$]/NaY = 0.05, (d) [Msim][$FeCl_4$]/NaY = 0.1, (e) [Msim][$FeCl_4$]/NaY = 0.2, (f) [Msim][$FeCl_4$]/NaY = 0.5, (g) [Msim][$FeCl_4$]/NaY = 1.

spectrophotometer. The thermogravimetric (TGA) analysis of the three solid acids was performed on Shimadzu TGA 50 instrument. All elemental analyses were obtained from PerkinElmer 20 analyzer. Melting points were recorded on a Buchi-560 apparatus. The amount of Fe present in the used catalyst composite was determined with an ICP-OES Perkin Elmer Optima 2100DV instrument. The laser micro-Raman spectroscopic measurement was conducted in a Horiba LabRAM HR spectrometer equipped with a He—Ne laser that has an excitation wavelength of 514.5 nm. The BET surface area of the catalysts was measured in Quantachrome Nova Win apparatus. The scanning electron microscopy (SEM) analyses were carried out using a JEOL JSM-6390LV SEM, equipped with an Energy-Dispersive X-ray analyzer.

2.2. Synthesis of NaY supported hybrid catalysts of [Msim][$FeCl_4$](**b–g**)

[Msim][$FeCl_4$] ionic solid was prepared through a reported procedure [5]. The [Msim][$FeCl_4$] loaded NaY zeolite catalysts were prepared by wet impregnation method. The following steps have been utilized: (i) the NaY zeolite powder was out gassed at 600 °C for 3 h, (ii) [Msim][$FeCl_4$] and NaY zeolite were mixed well with six different weight/weight (w/w) ratios (such as 0.03, 0.05, 0.1, 0.2, 0.5 & 1) of ionic solid and NaY zeolite using few drops of distilled EtOAc to ensure complete mixing, and finally (iii) the mixtures were heated at 150 °C in a vacuum oven for 12 h.

2.3. General procedure for the synthesis of 2-amino-4-arylpyrimidine derivatives **5**

A mixture of ethyl acetoacetate (1 mmol), aromatic aldehyde (1 mmol) and urea (1.5 mmol) was heated in a two necked 50 mL round bottom flask at 60 °C for 10 min using 3 mg of [Msim][$FeCl_4$]/NaY = 0.1 catalyst. The formation of 3,4-dihydropyrimidin-2-(1H)-one was confirmed through thin layer chromatography (TLC) using EtOAc and hexane (1:3) as solvent system. After completion of the 1st step, 1 mmol of 2,4-dinitrophenylhydrazine was added to the crude mixture along with few drops of dichloromethane and heated at 80 °C for the specified time. The progress of 2nd step was also tracked with TLC technique using EtOAc and hexane (1:5) as developing solvent. The work-up step involved addition of 6 mL of CH_2Cl_2 to the crude mixture to separate the unreacted DHPMs and catalyst by filtration from the solution of crude pyrimidine. The catalyst was recovered as solid residue on filter paper from the hot solution of DHPMs in ethanol. The saturation of dichloromethane (DCM) solution of pyrimidine at 0 °C precipitated the unreacted 2,4-dinitro-phenyl hydrazine as red precipitates. Evaporation of DCM solution yielded the pyrimidine derivatives as solid residue which was further recrystallized from acetone and methanol solution.

3. Results and discussion

3.1. Characterization of the hybrid catalysts

3.1.1. Powder XRD analysis

The powder XRD patterns of NaY and modified zeolite composites (Fig. 2) support the preservation of zeolite framework up to the w/w ratio of 0.2. Above that, complete destruction of the framework occurs which can be attributed for acid induced dealumination of Y- zeolite at 150 °C to maximum amount of extra framework aluminium species (EFAl) in presence of higher loaded (0.5 & 1) —SO_3H containing [Msim][$FeCl_4$] ionic solid [48–51].

A small peak observed at 2θ = 45.13° for all composites which becomes prominent for e (0.2), f (0.5) and g (1) composites. Partial ionic interaction between Fe species and zeolite framework could also occur during impregnation method and was found to be more effective beyond [Msim][$FeCl_4$]/NaY = 0.2 ratio. The extra peak centered at 2θ = 45.13° matches well with the XRD database of $FeCl_3$ (JCPDS card no. 770999) and represents the attachment of $[FeCl_4]^-$ species with the surface of zeolite. On modification, the crystallinity of the zeolite particles decreases and it has a direct correlation with loading percentages.

This implies that partial dealumination transforms a portion of crystalline zeolite into amorphous state along with preservation of significant fraction of crystalline structure in Fig. 2 up to 0.2 (e) loading of [Msim][$FeCl_4$] salt [52].

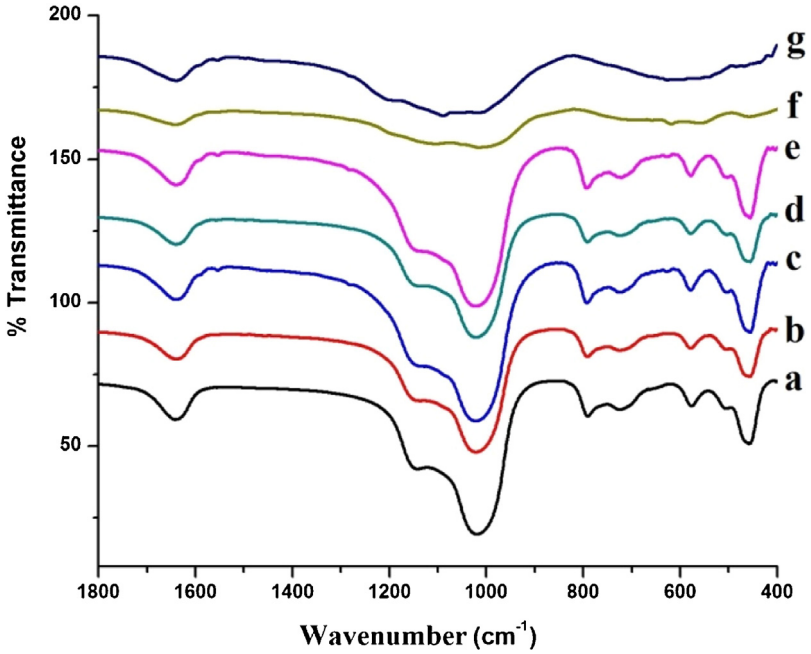

Fig. 3. FT-IR spectra of the parent as well as modified NaY zeolite samples, where (a) NaY, (b) [Msim][$FeCl_4$]/NaY = 0.03, (c) [Msim][$FeCl_4$]/NaY = 0.05, (d) [Msim][$FeCl_4$]/NaY = 0.1, (e) [Msim][$FeCl_4$]/NaY = 0.2, (f) [Msim][$FeCl_4$]/NaY = 0.5, (g) [Msim][$FeCl_4$]/NaY = 1.

The relative crystallinity difference between modified samples and the parent zeolite were compared by taking four high intensity peaks at 2θ = 15.3°, 23.48°, 26.85° and 31.05° and an informative graph is included in the supplementary section along with the table (see, supporting file, Fig. 1 and Table 1).

3.1.2. FT-IR analysis

FT-IR spectra of the parent and the modified samples were recorded and represented in Fig. 3 in the region 400–1800 cm^{-1}. The 0.2(e) loaded sample shows optimum dealumination state, without an appreciable change of basic vibrational frequencies of NaY zeolite like powder X-ray analysis (Fig. 2) [53]. The sharp band in the region of 1638–1642 cm^{-1} for all composites can be considered for bending vibration of water molecules attached to the zeolite structure including —C=N— stretching vibration of imidazolium cation of ionic salt [5]. The O—H stretching vibration at 3459 cm^{-1} for parent zeolite shifts its position to 3441 cm^{-1} with an intense peak for the composite [Msim][$FeCl_4$]/NaY = 1(g) and this represents the existence of strong hydrogen bonding within the composite involving O—H group [54]. The framework sensitive double-ring vibration peak at 577 cm^{-1} of NaY observed around 578–579 cm^{-1} for the composites of 0.03(b), 0.05(c), 0.1(d) and 0.2(e). The other characteristic frequencies of NaY zeolite, corresponding to bending, symmetrical and asymmetrical stretching vibrations of TO_4 (Si or Al) building units have been displayed at 455–458 cm^{-1}, 721–793 cm^{-1} and 1019–1143 cm^{-1} for the above four composites [55]. The strong S—O symmetric and asymmetric stretching and bending vibrations of ionic salt at 1222 cm^{-1}, 1075 cm^{-1} and 618 cm^{-1} are also overlapping with the above fundamental vibrations of TO_4 unit of NaY zeolite [5]. The characteristic absorption peaks of the composites almost disappeared for 0.5(f) and 1(g) [Msim][$FeCl_4$]/NaY samples which can be accounted for destruction of the parent zeolite framework by rapid acid mediated dealumination process in these two samples to form large amount of non-framework Al species such as $Al(OH)_2^+$ or AlO^+ etc [56,57].

From the above discussion of IR studies, we can assume that the modified samples have some extra framework species of aluminosilicate and silica gel formed by partial or complete destruction of the parent framework during preparation of [Msim][$FeCl_4$] loaded composites with NaY. Furthermore, the identical FT-IR spectra of four composites (b–e) and NaY(a) represents insufficient dealumination inside the framework in presence of less amount of acidic salt [58].

The recorded FT-IR spectra (Fig. 4) of [Msim][$FeCl_4$]/NaY = 0.1 sample after calcination at 250 °C, 350 °C and 450 °C also witnessed complete intactness of characteristic bands of the fresh 0.1(d) composite within 400–1800 cm^{-1}. This observation supports the thermal stability of this composite with small portion of non-framework Al species in solid state [59,60]. On the other hand, the intensity of O—H bending peaks gradually reduced at high temperature calcination which indicate the loss of some hydroxyls associated with the 1641 cm^{-1} band up to 450 °C as included in supporting information (Fig. 3, Supporting File).

3.1.3. SEM-EDX analysis

Fig. 5 displays the SEM images of NaY zeolite, 0.1(d) and 0.2(e) [Msim][$FeCl_4$]/NaY composites. Both the size and uniformity of the particles decrease on modification. Originally the parent NaY zeolite has cube like large particle structure. The change in surface morphology for the loaded materials depicts the anchoring of ionic solid on the surface of zeolite as smaller size cube type particles. They form more aggregation in case of w/w ratio of 0.2 than 0.1. This may convert the surface of [Msim][$FeCl_4$]/NaY = 0.2 composite to non-uniform in nature and decreases the number of acidic sites for catalytic performance.

The EDX spectra of the [Msim][$FeCl_4$]/NaY = 0.1 composite confirmed the presence of constituent elements of the ionic solid along with the zeolite (Fig. 6).

3.1.4. TEM analysis

The TEM imaging was carried out for the [Msim][$FeCl_4$]/NaY = 0.1 composite zeolite at high resolution (Fig. 7). These images proved that in the composite the crystallinity of basic NaY zeolite was preserved as observed in the PXRD pattern in Fig. 2. No substantial damages were detected on the hexagonal

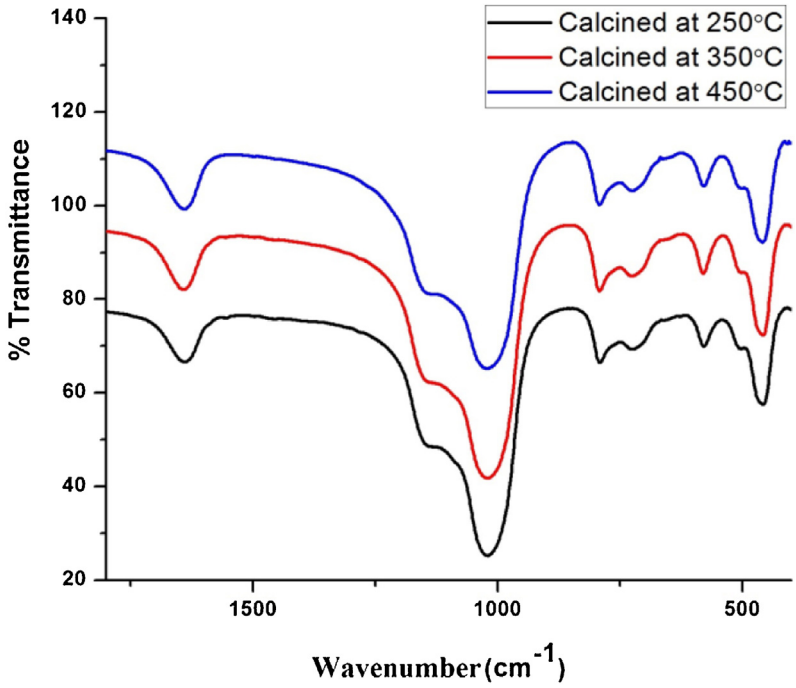

Fig. 4. FT-IR spectra of the sample; [Msim][$FeCl_4$]/NaY = 0.1 calcined at 250 °C, 350 °C and 450 °C.

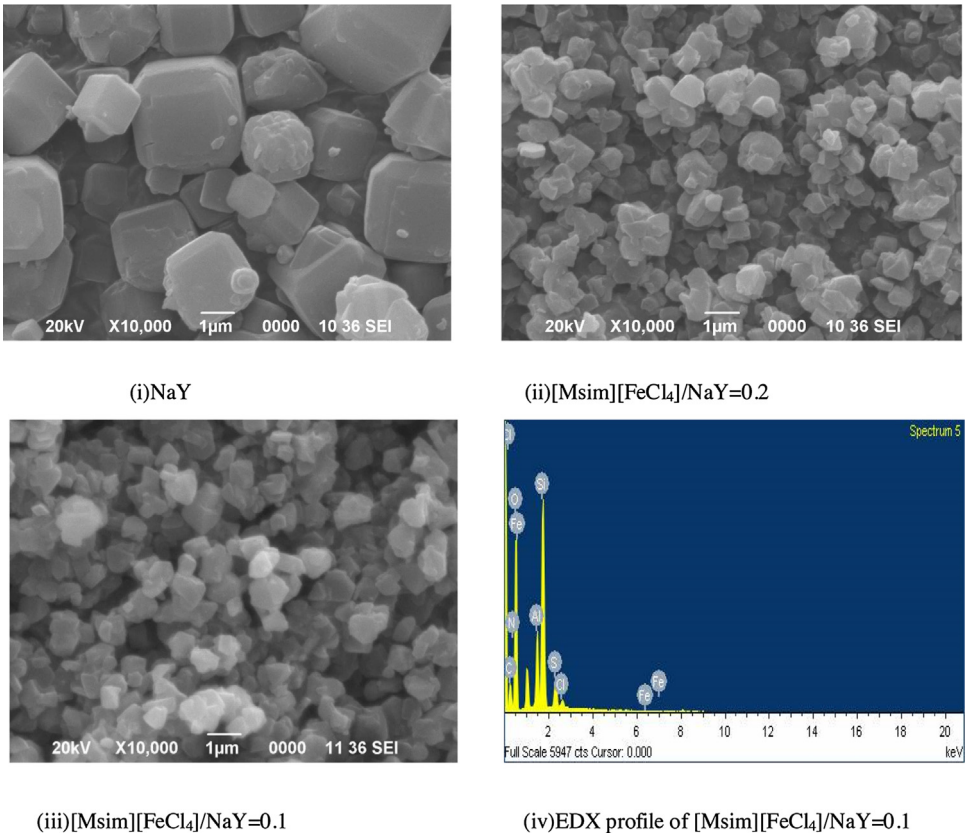

Fig. 5. SEM images of (i) NaY, (ii) [Msim][$FeCl_4$]/NaY = 0.2, (iii) [Msim][$FeCl_4$]/NaY = 0.1, (iv) EDX profile for [Msim][$FeCl_4$]/NaY = 0.1 composite.

structure of NaY zeolite [61]. The TEM images also supported the accumulation of [Msim][$FeCl_4$] salt as clusters on the external surface of zeolite in (c) and (d) similar to the SEM images (Fig. 5).

3.1.5. *BET analysis*

Table 1 shows the BET surface area and pore volumes of NaY and four [Msim][$FeCl_4$]/NaY composites. The composites displayed abrupt decrease of surface area as compared to NaY. This may be attributed to mostly non-porous coverage of zeolite surface by the

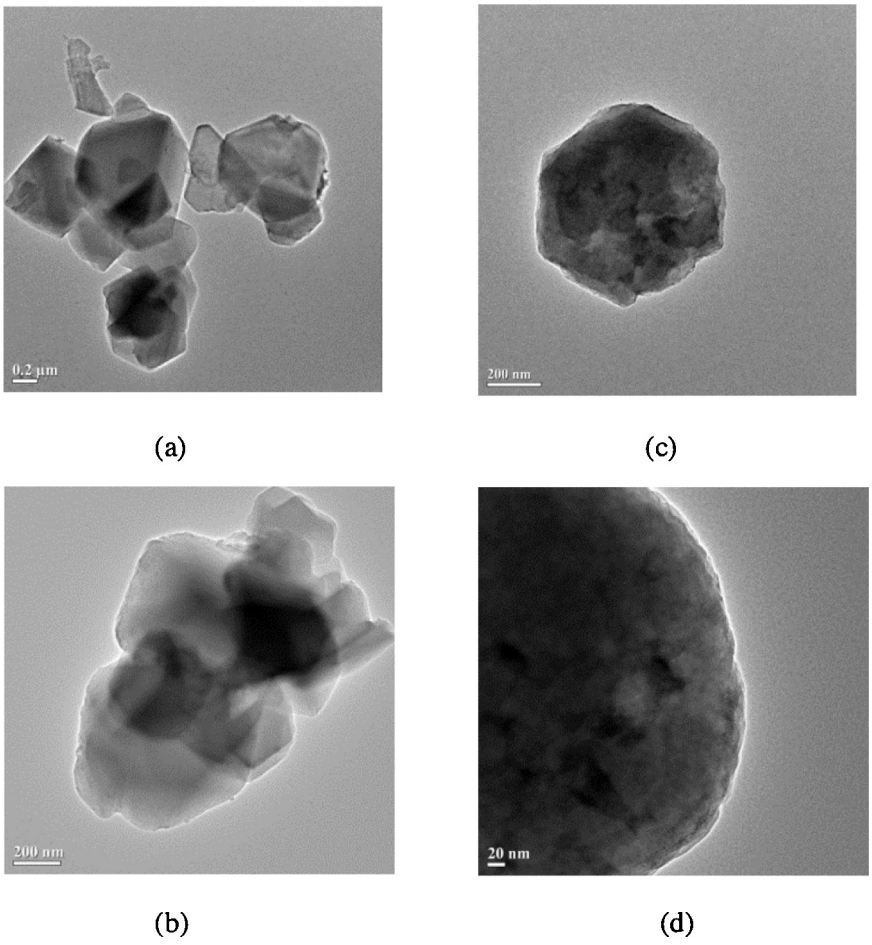

Fig. 6. TEM images of [Msim][$FeCl_4$]/NaY = 0.1 composite.

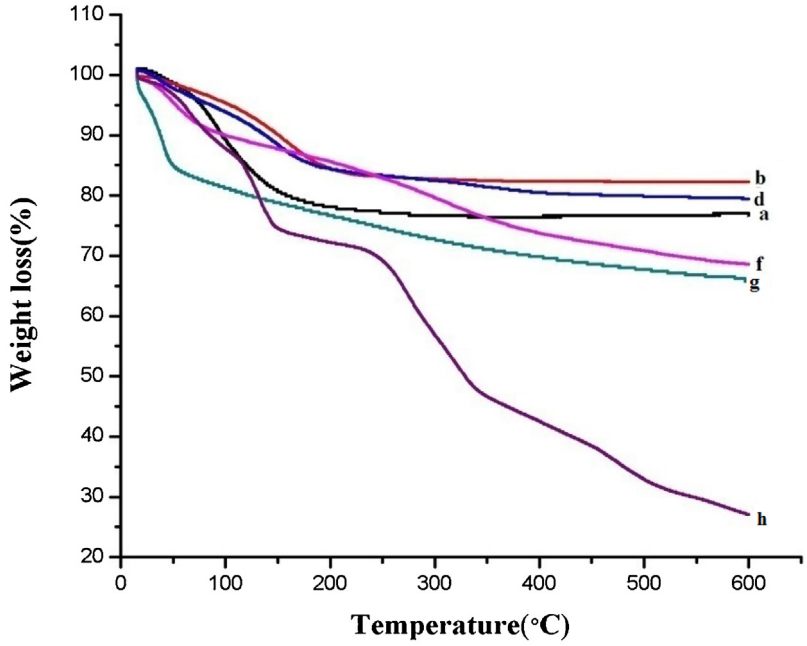

Fig. 7. TGA profiles of parent zeolite and modified samples: (a) NaY; (b) [Msim][$FeCl_4$]/NaY = 0.03; (d) [Msim][$FeCl_4$]/NaY = 0.1; (f) [Msim][$FeCl_4$]/NaY = 0.5; (g) [Msim][$FeCl_4$]/NaY = 1; (h) [Msim][$FeCl_4$].

Table 1
Textural properties of NaY and the composites.

Sl no	Sample name	Surface area(m^2/g)	Pore Volume(cm^3/g)
1	NaY	900	0.324
2	[Msim][$FeCl_4$]/NaY = 0.03	9	0.009
3	[Msim][$FeCl_4$]/NaY = 0.05	16	0.011
4	[Msim][$FeCl_4$]/NaY = 0.1	30	0.016
5	[Msim][$FeCl_4$]/NaY = 0.2	38	0.030

ionic solid and can lead to restricted access to the zeolite pores for adsorption of N_2 gas. Interestingly, we also observed opposite trend for gradual increase of surface area and pore volume with increase in the percentage loading (entry 2–5, Table 1). This trend can be supported by the phenomenon of more clustering of ionic solid on the zeolite surface as the loading increases, which was also further confirmed from SEM photograph (Fig. 5). Such type of clusters formation may create some porous host points into which the N_2 gas prefer to adsorb and thus it was reflected as increasing surface area in BET analysis in Table 1 against increase in the loading of ionic solid [62].

3.1.6. TGA analysis

Thermogravimetric analysis was conducted to compare the overall thermal stability of NaY, [Msim][$FeCl_4$] and various composites of [Msim][$FeCl_4$]/NaY (Fig. 7). The small weight loss steps of NaY(a) and the composite materials 0.03(b) and 0.1(d) around 200 °C can be assigned to elimination of physisorbed or bound water attached to Na^+ of the parent framework (or hydrated cation for the modified samples) [63]. The amount of such water is more for the NaY (a) framework. For (b) and (d) samples, the number of Al content slightly decreases through partial exchange of proton with Na^+ which converts only a small fraction of the crystalline structure into non- framework Al structure due to lower percentage of —SO_3H functionalized [Msim][$FeCl_4$] salt. It was found in some observation that appearance of EFAl brings a stabilizing effect to the modified zeolite framework by healing of Al defects with migrating H_4SiO_4 molecules [64].

Therefore, as compared to the parent zeolite, the modified samples (b & d) display smaller weight loss up to 200 °C. The moderate release of water molecule for 0.1 (d) composite with partial change of the basic TO_4 frequencies (Fig. 3) can also be evidenced from the comparative O—H bending vibration peak intensity observation at high temperature calcinations (see Fig. 3, Supporting file). Above 200 °C no significant weight loss was observed for these two samples 0.03(b) and 0.1(d) which can be speculated for probable ionic interaction of $FeCl_4^-$ anion complex of Na^+ exchanged ionic salt with partial Lewis acidic sites of the extra framework species such as $Al^+(OH)_2$. As the loading of ionic solid increases from 0.5 (f) to 1 (g), the weight loss below 100 °C becomes rapid (approximately 15%) for the composite 1(g). At the same time, this composite expresses its framework structure as the highest dealumination state in the PXRD and FT-IR patterns, so we cannot exclude the possibility of water loss below 100 °C both from the hydrated cations and dehydroxylation of Al defects consisting of four silanols (Si—OH)[65]. The loss of water at 50 °C for the above sample (g) was further confirmed from the sudden drop of peak intensity for O—H stretching vibration with two calcined samples at 50 °C and 100 °C (See Fig. 4, Supporting file). The two onset decomposition points for [Msim][$FeCl_4$] ionic solid at 115–150 °C are enhanced to 170 °C in case of (b) and (d) and it raised to 200 °C for (f). The composite (f) witnessed gradual weight loss from 200 °C to 600 °C.

3.1.7. Raman analysis

The Raman spectra for NaY and three composites are presented in Fig. 8. The most intense peak for NaY zeolite was detected at

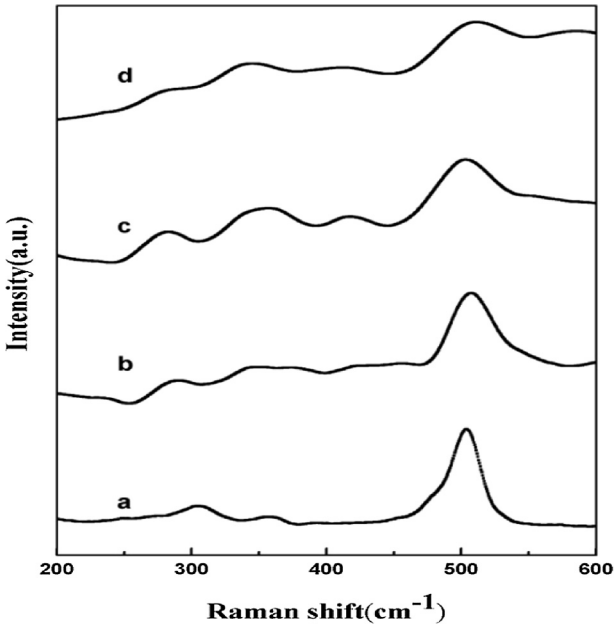

Fig. 8. Comparison of the Raman spectra of (a) NaY; (b) [Msim][$FeCl_4$]/NaY = 0.03; (c) [Msim][$FeCl_4$]/NaY = 0.05; (d) [Msim][$FeCl_4$]/NaY = 0.2.

Table 2
Calculation of the Hammett Function of the modified zeolite samples with equal concentration of composites and indicator.

Entry	Sample name[a]	A_{max}	[I]%	[IH]%	H_0
1.	Blank	2.493	100	0	–
2.	[Msim][$FeCl_4$]/NaY = 0.03	1.256	50.4	49.6	0.997
3.	[Msim][$FeCl_4$]/NaY = 0.05	1.244	49.9	50.1	0.988
4.	[Msim][$FeCl_4$]/NaY = 0.1	1.209	48.49	51.51	0.964
5.	[Msim][$FeCl_4$]/NaY = 0.2	1.311	52.59	47.40	1.035

[a] Indicator: 4-nitroaniline.

500 cm^{-1} and is characteristics of the T—O—T bending vibration where T denotes Si or Al atoms of zeolite frameworks [66,67]. For the composites, a broad shoulder at 337–341 cm^{-1} was detected, which is exclusive proof of the presence of the ionic solid on the NaY zeolite surface [5]. The shoulder goes prominent with increase in loading.

3.1.8. Acidity determination by Hammett plot

The relative acidity of the composites was determined on an UV–vis spectrophotometer with Hammett plots (Fig. 9A–C) using *p*-nitroaniline as the basic indicator [68]. The absorbance of the indicator [I] in the composite solutions was reduced as the acidity of the catalysts increases. The lower molar absorptivity of protonated form $[HI]^+$ of the indicator didn't show any absorption. The Hammett functions H° of various composite materials were calculated from the absorption differences $[I]/[IH]^+$ using equation-1 (Table 2).

$$H^\circ = pK(I)aq + \log[I]/[IH]^+ \qquad (1)$$

where p*K*(I)aq is the p*K*a value of the *p*-nitroaniline indicator in aqueous solution. The procedure required the mixing of equal concentration of 4-nitroaniline (5 mg/L, p*K*a = 0.99) and catalyst (equal amounts of all) in ethanol solution. The indicator observed maximum absorbance at 378 nm in ethanol. The Hammett plot expressed the following decreasing acidity order of the four modified zeolite samples against their observed H° values as (Table 2): [Msim][$FeCl_4$]/NaY = 0.1(d) > [Msim][$FeCl_4$]/NaY = 0.05(c) >Msim][$FeCl_4$]/NaY = 0.03(b) > [Msim][$FeCl_4$]/NaY = 0.2(e). The formation

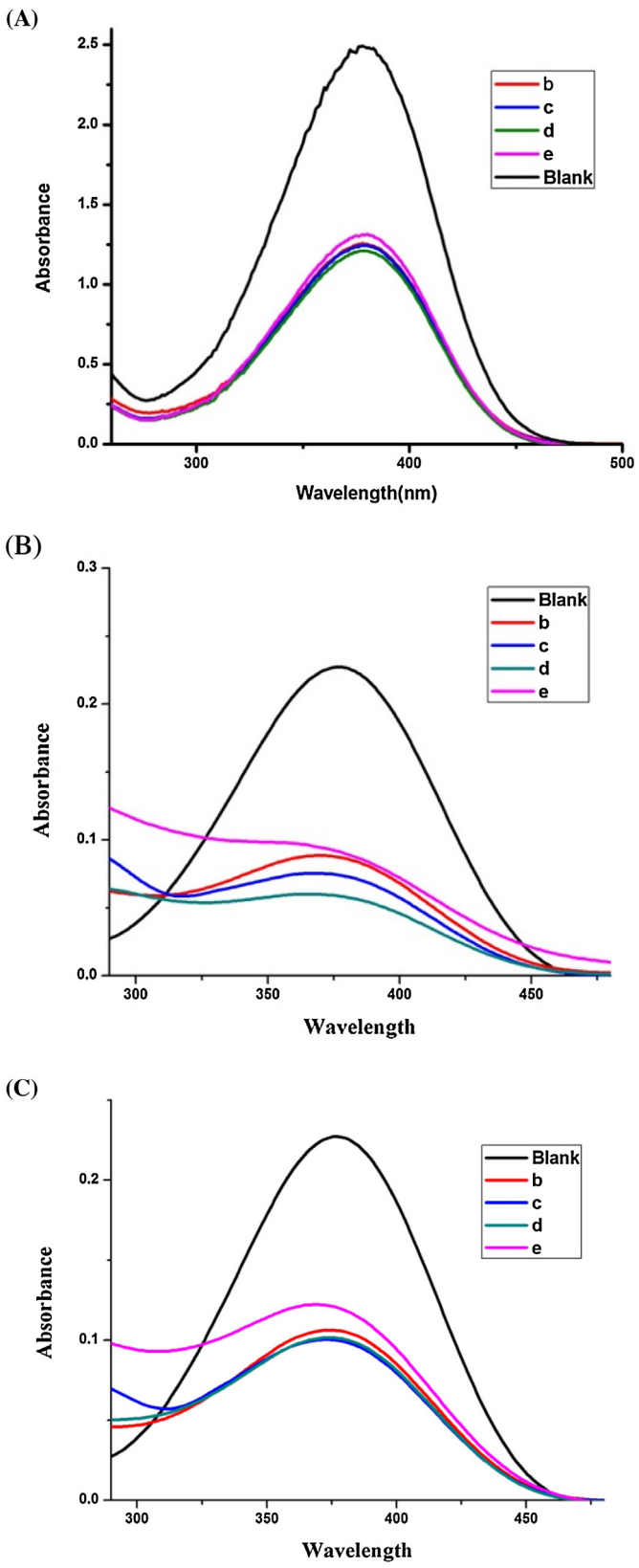

Fig. 9. (A) Hammett plots of the hybrid materials of zeolite samples by mixing equal concentration of indicator and composites: (B) [Msim][FeCl4]/NaY = 0.03 ; (C) [Msim][FeCl4]/NaY = 0.05; (D) [Msim][FeCl4]/NaY = 0.1; (E) [Msim][FeCl4]/NaY = 0.2. (B) Hammett plots of the hybrid materials of zeolite samples by mixing 1: 4 ratio of indicator and composites (C) Hammett plots of the hybrid materials of zeolite samples by mixing 2:3 ratio of indicator and composites.

of more clusters in case of (e) as supported by SEM analysis may block the active sites of the composites for interaction with the basic indicator and it leads to decrease in the acidity of (e) as compared to (d). The powder XRD profile also indicates the destruction of the zeolite structure above w/w ratio of 0.2.

To determine the effect of composite concentration on Hammett acidity, we also evaluated the acidity of the four composites in two different ratios (1:4 and 2:3) by altering the concentration of *p*-nitroaniline and composites respectively which produced two identical Hammett plots (Fig. 9B and C). Both the plots revealed the same acidity order as observed from the Hammett plot (Table 2**)** of equal concentration of the composites and indicator. With increasing concentrations of the composites the unprotonated form of the basic indicator showed lower absorbance values.

3.2. Catalytic performance

3.2.1. Optimization of the reaction condition

The acidic scale of the four composites with w/w ratio up to 0.2 has been determined through the Hammett plot. Due to small difference in acidity, we decided to test the catalytic activity of all of them. From the time frame required for completion of the reaction, the [Msim][$FeCl_4$]/NaY = 0.1 hybrid composite was chosen as the best acidic catalyst for the two-step one pot model synthesis of pyrimidine derivatives via *in situ* generation of Biginelli DHPMs from three component reaction of ethyl acetoacetate (1 mmol), benzaldehyde (1 mmol) and urea (1.5 mmol) followed by reaction with 2,4-dinitrophenyl hydrazine (1 mmol) (Table 3, entries 1–4). The catalytic activity of the composite was tested by varying the amount of catalyst (3/5/10/15 mg) at 60 °C in neat condition. Irrespective of the amounts of the catalyst, the first step of reaction completed within 5–10 min without solvent at 60 °C as monitored by TLC plate (Table 3, entries 3, 5–7). By conducting the reaction at room temperature, it has been observed that only 3 mg of catalyst is sufficient to produce 3,4-dihydropyrimidinone exclusively in 30 min (Table 3, entry 8). However, no product formation was observed for the second step at room temperature. At 60 °C, 65–75% yield was observed for the second step in around 5–25 min duration using different amounts of the catalyst (3/5/10/15 mg) (Table 3, entries 3, 5–7). Therefore, we decided to carry out the 2nd step at 80 °C and it gave improved result. Almost 87% yield was observed in 10 min (Table 3, entry 8). We have also checked the utility of this catalytic system for industrial scale reactions by performing the same reaction on 20 mmol scale. We are pleased to report here that the composite was able to maintain its activity at that scale under the optimized conditions and has successfully completed the reaction within 10 min in 2nd step.

3.2.2. Substrate study and plausible mechanism for the sequential conversion of DHPMs to 2-amino-4-arylpyrimidines **5**

By utilising the above optimized conditions, various pyrimidine derivatives were synthesized from 3,4-dihydropyrimidinone derivatives obtained through the three component reaction of various aryl aldehydes with ethyl acetoacetate and urea and then condensation with 2,4-dinitro phenylhydrazine in acidic medium at high temperature. These results are included in Table 4. From this table, we can infer that the nature of various electron donating or withdrawing group containing aryl group at C-4 position of 3,4-dihydropyrimidinones didn't influence the reaction rate. All the reactions yielded 80–87% of pyrimidine product in 2nd step within 10–15 min at 80 °C. The 2nd step may proceed through activation of carbonyl group for condensation with 2,4-dinitro phenyl hydrazine in presence of the acid catalyst to form the hydrazone derivatives as reaction intermediate (Scheme 2). Under the reaction condition, this intermediate can undergo acid catalysed

Table 3
Optimization study for the one pot synthesis of pyrimidine derivatives.

Entry	Catalyst	Amount of the catalyst(mg)	1st step	2nd step	%Yield[a]
			Time(min)	Time(min)	**5a**
1.	[Msim][$FeCl_4$]/NaY = 0.03	15	7	10	72
2.	[Msim][$FeCl_4$]/NaY = 0.05	15	5	10	73
3.	[Msim][$FeCl_4$]/NaY = 0.1	15	3	5	75
4.	[Msim][$FeCl_4$]/NaY = 0.2	15	10	15	70
5.	[Msim][$FeCl_4$]/NaY = 0.1	10	5	12	70
6.	–do-	5	10	20	68
7.	–do-	3	10	25	65
8.	–do-	3	30	10	87[b]

[a] Reactions were conducted at 60 °C for entries 1–7 in each step.
[b] The 1st step was performed at room temperature and 2nd step at 80 °C for entry 8.

Table 4
Synthesis of pyrimidine derivatives using [Msim][$FeCl_4$]/NaY = 0.1 composite as catalyst.

Entry	Aldehyde **2**	Time(min)		Yield (%) **5**	M.p.°C **5**
		Step-I [a] **4**	Step-II [b] **5**		
1	C_6H_5 **2a**	10	10	87 **5a**	214.7–217.3
2	4-$MeOC_6H_4$ **2b**	15	10	84 **5b**	204.8–207.2
3	4-$NO_2C_6H_4$ **2c**	10	10	82 **5c**	215.4–217.5
4	4-MeC_6H_4 **2d**	15	10	85 **5d**	227.6–229.4
5	2-Naphthyl **2e**	20	10	80 **5e**	163.1–164.0
6	4-HOC_6H_4 **2f**	10	10	83 **5f**	97.4–97.9
7	3,4,5-$(MeO)_3$ C_6H_2 **2g**	10	10	82 **5g**	158.1–160.5

[a] Reactions were performed at 60 °C using 3 mg of 0.1 composite as catalyst with the mixture of ethyl acetoacetate(**1**), aromatic aldehyde(**2**) and urea(**3**).
[b] 2,4-Dinitrophenyl hydrazine was added and heated the crude mixture at 80 °C.

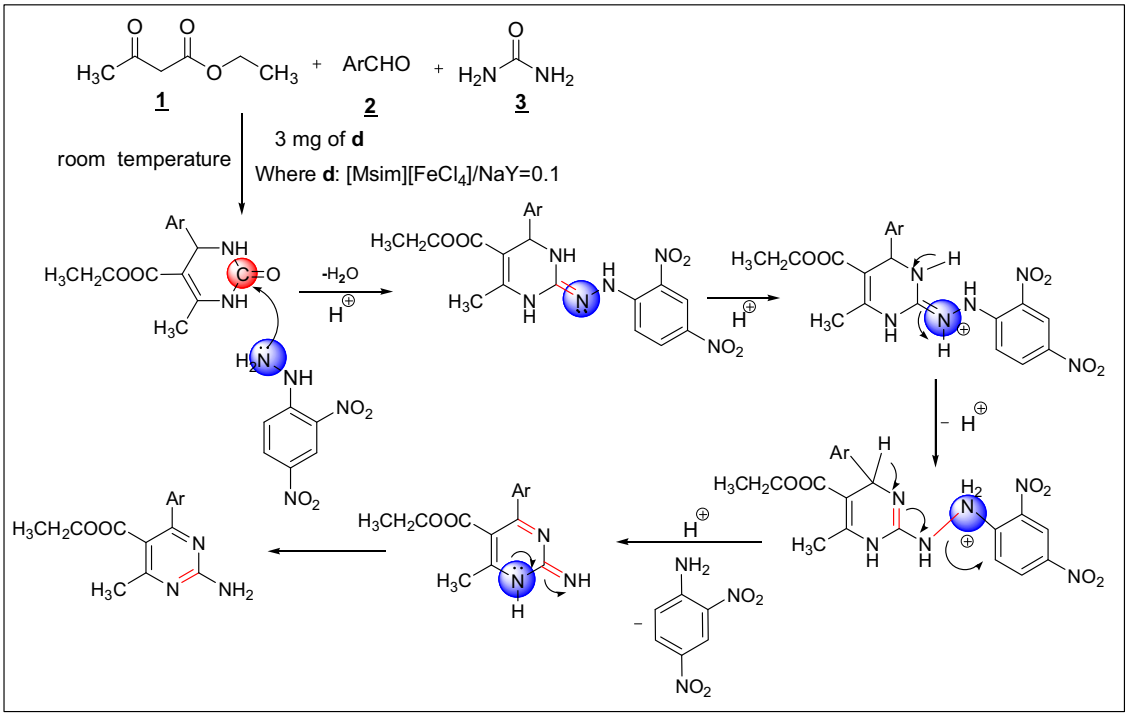

Scheme 2. Proposed mechanisms for one step conversion of Biginelli pyrimidin-2-(*1H*)-one to 2-amino-4-aryl pyrimidine.

aromatization reaction to 2-amino-pyrimidine derivatives with expulsion of 2,4-dinitroaniline as side product.

3.2.3. *Spectral analysis of 2-amino-4-aryl pyrimidine derivatives* ***5***

The structures of new 2-amino-4-aryl pyrimidines **5** were confirmed from the ^{1}HNMR, ^{13}CNMR, FT-IR and CHN elemental analysis data. Furthermore, two pyrimidines **5a** and **5d** were further studied with COSY, HETCOR and DEPT techniques. All these spectral analysis data have been included as supporting information in the supplementary file.

3.2.4. *Recycling of catalyst*

The stability of the active species in supported catalysts is of great concern. The reusability of [Msim][$FeCl_4$]/NaY = 0.1 composite as catalyst was investigated for the one pot synthesis of **5a** under

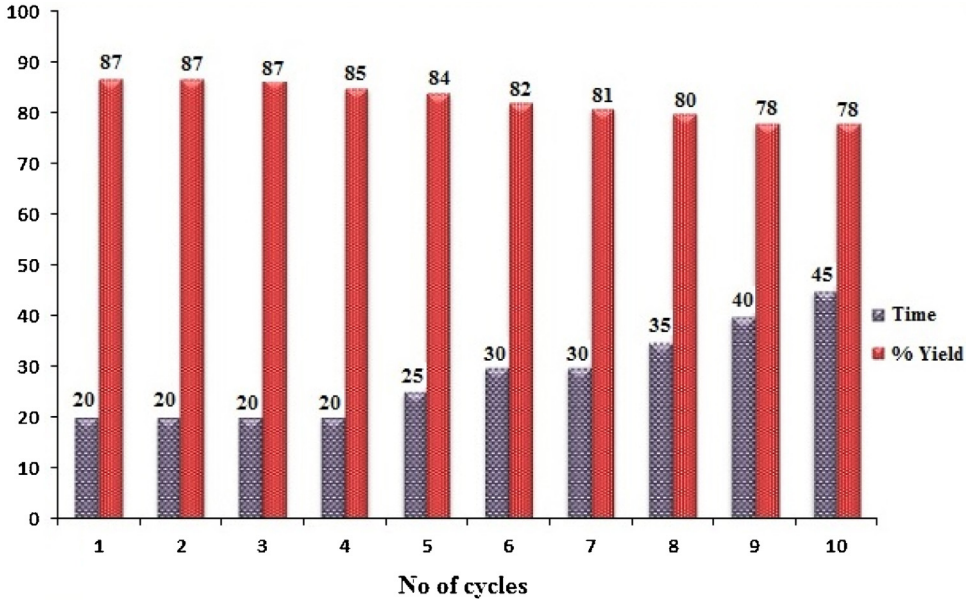

Fig. 10. Reusability profile of [Msim][$FeCl_4$]/NaY = 0.1 composite.

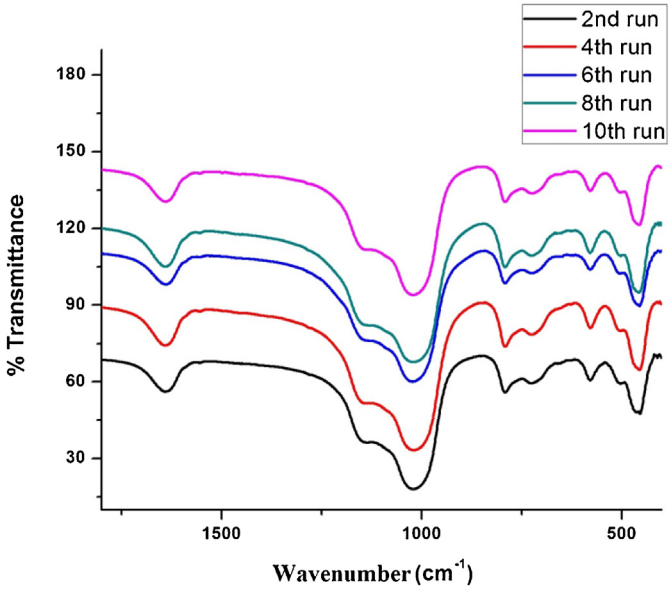

Fig. 11. FT-IR spectra of the used catalyst from 2nd cycle onwards after every alternate cycle.

the optimized conditions on a 5 mmol scale reaction. The filtered catalyst was repeatedly washed with hot EtOH to make it free from traces of the reaction mixture and then reactivated in vacuum oven at 100 °C for 3 h. The reusability was found to be quite good and it could be reused up to ten consecutive cycles (Fig. 10) with moderate loss in activity.

3.2.5. Characterization of the used catalyst

The integrity of the used catalyst was checked through FT-IR, Raman spectra and ICP-OES from 2nd cycle onwards after every alternate cycle. FT-IR spectra of the reused catalyst after every alternate cycle from 2nd cycle onwards showed clear evidence of the presence of characteristic bands of the parent zeolite structure as well as the guest ionic solid species (Fig. 11).

However, the peak characteristic of double ring vibration at 577 cm^{-1} for the reused catalyst also shifted slowly towards higher values around 579 cm^{-1} from 2nd cycle onwards as tabulated in the supporting material (see, Tabel 3 in supporting file). From this table, we determined the Si/Al ratio of used [Msim][$FeCl_4$]/NaY = 0.1 catalyst from 2nd alternate cycle (see, Table 3 in supporting file) using the IR double-ring (υ_{DR}) vibration values to the empirical relation given by Rüscher et al. [69] with Si/Al = (1-x)/x.

$$x = 3.857 - 0.00619\upsilon_{DR}(cm^{-1}) \qquad (2)$$

This table showed the slow leaching of some non-framework Al species to the solution during repeated washing with hot ethanol and then reactivation in vacuum at 100 °C for several hour up to ten consecutive runs. Simultaneously, the ICP-OES results (Table 5) also indicated slight loss of Fe content in every alternate cycle after 2nd run from the complex anion $FeCl_4^-$. The leaching of some non-framework Al species may destabilize the ionic interaction of $FeCl_4^-$ anion with the Lewis acidic site of composite framework. As results, the attached $FeCl_4^-$ anion leaches out from the composite to the solution.

Table 5
ICP-OES results of the used catalysts.

Entry	Cycles	Amount of Fe(mg/L)
1.	2nd cycle	10.23
2.	4th cycle	9.31
3.	6th cycle	7.32
4.	8th cycle	6.92
5.	10th cycle	6.64

Raman spectra for the spent catalyst are included in the supporting file. The intensity of the broad peak at 351 cm^{-1} indicative of $FeCl_4^-$ species gradually decreases towards the 10th cycle. It clearly agrees with the leaching information obtained from the ICP-OES study. The respective characterization techniques of the spent catalyst supports the recyclability profile Fig. 10 of [Msim][$FeCl_4$]/NaY = 0.1 composite.

4. Conclusions

The hybrid composites were characterized with different analytical techniques and they denote the successful entrapment of the ionic solid particles above the NaY zeolite surface. The composite materials are superior in some respects like thermal stability,

recyclability etc. than the sole ionic solid. They synergistically combine the advantages of both the host and guest components. The [Msim][$FeCl_4$]/NaY = 0.1 composite exhibited excellent catalytic activity towards the sequential three component two step conversion of 3,4-dihydropyrimidin-2(*1H*)-one to multifunctionalized 2-amino-4-arylpyrimidines. The present methodology is a novel efficient route towards the development of pyrimidines in less time and would be applicable for the library synthesis of 2-amino-4-arylpyrimidine derivatives without using any oxidizing agents and solvents with easy purification. The 0.1 ratio composite material showed good catalytic activity up to ten consecutive cycles in solvent-free medium under the optimized reaction condition.

Acknowledgement

The authors are thankful to Sophisticated Analytical Instrumentation Centre, Tezpur University for analyses of various samples for this work.

Appendix A. Supplementary data

Supplementary data associated with this article can be found, in the online version, at http://dx.doi.org/10.1016/j.apcata.2016.06.015.

References

[1] T. Selvam, A. Machoke, W. Schwieger, Appl. Catal. A: Gen. 445–446 (2012) 92–101.
[2] S. Ntais, A.M. Moschovi, F. Paloukis, S. Neophytides, V.N. Burganos, J. Power Sources 196 (2011) 2202–2210.
[3] K. Arya, D.S. Rawat, H. Sasai, Green Chem. 14 (2012) 1956–1963.
[4] V.I. Pârvulescu, C. Hardacre, Chem. Rev. 107 (2007) 2615–2665.
[5] P. Gogoi, A.K. Dutta, P. Sarma, R. Borah, Appl. Catal. A: Gen. 492 (2015) 133–139.
[6] Q. Zhang, J.M. Shreeve, Chem. Rev. 114 (2014) 10527–10574.
[7] M.A.P. Martins, C.P. Frizzo, D.N. Moreira, N. Zanatta, H.G. Bonacorso, Chem. Rev. 108 (2008) 2015–2050.
[8] T.L. Greaves, C.J. Drummond, Chem. Rev. 108 (2008) 206–237.
[9] L.A. Banchard, D. Hancu, E.J. Beckman, J.F. Brennecke, Nature 399 (1999) 28.
[10] P. Wasserscheid, T. Welton, Ionic Liquids in Synthesis, vol. 2, 2nd ed., Wiley-VCH, 2003.
[11] D. Zhao, M. Wu, Y. Kou, E. Min, Catal. Today 74 (2002) 157–189.
[12] R.F. de Souza, J.C. Padilha, R.S. Goncalves, J. Dupont, Electrochem. Commun. 5 (2003) 728–731.
[13] S.Y. Lee, A. Ogawa, M. Kanno, H. Nakamoto, T. Yasuda, M. Watanabe, J. Am. Chem. Soc. 132 (2010) 9764–9773.
[14] C. DeCastro, E. Sauvage, M.H. Valkenberg, W.F. Holderich, J. Catal. 196 (2000) 86–94.
[15] M.H. Valkenberg, C. DeCastro, W.F. Holderich, Green Chem. 4 (2002) 88–93.
[16] A. Eguizábala, J. Lemus, M. Urbiztondo, A.M. Moschovi, S. Ntais, J. Soler, M.P. Pina, J. Power Sources 196 (2011) 4314–4323.
[17] B. Xinab, J. Hao, Chem. Soc. Rev. 43 (2014) 7171–7187.
[18] R. Fehrmann, A. Riisager, M. Haumann, Supported Ionic Liquids: Fundamentals and Applications, Wiley VCH, 2014.
[19] A.E. Amr, A.M. Mohamed, S.F. Mohamed, N.A. Abdel-Hafez, A.G. Hamman, Bioorg. Med. Chem. 14 (2006) 5481–5488.
[20] M.M. Ghorab, F.A. Ragab, S.I. Alqasoumi, A.M. Alafeefy, S.A. Aboulmagd, Eur. J. Med. Chem. 45 (2010) 171–178.
[21] S.N. Darandale, D.N. Pansare, N.A. Mulla, D.B. Shinde, Bioorg. Med. Chem. Lett. 23 (2013) 2632–2635.
[22] S. Nagarajan, P. Shanmugavelan, M. Sathishkumar, R. Selvi, A. Ponnuswamy, H. Harikrishnan, V. Shanmugaiah, S. Murugavel, Bioorg. Med. Chem. Lett. 24 (2014) 4999–5007.
[23] M. Matloobi, C.O. Kappe, J. Comb. Chem. 9 (2007) 275–284.
[24] M. Watanabe, H. Koike, T. Ishiba, T. Okada, S. Seo, K. Hirai, Bioorg. Med. Chem. 5 (1997) 437–444.
[25] A. Rajacka, K. Yuvarajua, C. Praveena, Y.L.N. Murthya, J. Mol. Catal. A: Chem. 370 (2013) 197–204.
[26] L.M. Ramos, A.Y.P. de Leon y Tobio, M.R. dos Santos, H.C.B. de Oliveira, A.F. Gomes, F.C. Gozzo, A.L. de Oliveira, B.A.D. Neto, J. Org. Chem. 77 (2012) 10184–10193.
[27] L. Zhang, Z. Zhang, Q. Liu, T. Liu, G. Zhang, J. Org. Chem. 79 (2014) 2281–2288.
[28] P.K. Sahu, P.K. Sahu, D.D. Agarwal, RSC Adv. 3 (2013) 9854–9864.
[29] J.H. Clark, D.J. Macquarrie, J. Sherwood, Chem. Eur. J. 19 (2013) 5174–5182.
[30] J. Safari, Z. Zarnegar, New J. Chem. 38 (2014) 358–365.
[31] H.G.O. Alvim, T.B. de Lima, H.C.B. de Oliveira, F.C. Gozzo, J.L. de Macedo, P.V. Abdelnur, W.A. Silva, B.A.D. Neto, ACS Catal. 3 (2013) 1420–1430.
[32] H.G.O. Alvim, T.B. Lima, A.L. de Oliveira, H.C.B. de Oliveira, F.M. Silva, F.C. Gozzo, R.Y. Souza, W.A. da Silva, B.A.D. Neto, J. Org. Chem. 79 (2014) 3383–3397.
[33] A. Wang, X. Liu, Z. Su, H. Jing, Catal. Sci. Technol. 4 (2014) 71–80.
[34] C.O. Kappe, Tetrahedron 49 (1993) 6937–6963.
[35] J.J.V. Eynde, N. Audiart, V. Canonne, S. Michel, Y. Van Haverbeke, C.O. Kappe, Heterocyclic 45 (1997) 1967–1978.
[36] C.O. Kappe, P. Roschger, J. Heterocycl. Chem. 26 (1989) 55–64.
[37] A. Puchala, F. Belaj, J. Bergman, C.O. Kappe, J. Heterocycl. Chem. 38 (2001) 1345–1352.
[38] P. Shanmugam, P.T. Perumal, Tetrahedron 62 (2006) 9726–9734.
[39] K. Yamamoto, Y.G. Chen, F.G. Buono, Org. Lett. 7 (2005) 4673–4676.
[40] M.S. Akhtan, M. Seth, A.P. Bhaduri, Indian J. Chem. 26B (1987) 556–561.
[41] N.N. Karade, S.V. Gampawar, N.P. Tale, S.B. Kedar, J. Heterocycl. Chem. 47 (2010) 740–744.
[42] Z.-J. Quan, Y. Lv, Z.-J. Wang, Z. Zhang, Y.-X. Da, X.-C. Wang, Tetrahedron Lett. 54 (2013) 1884–1887.
[43] F.A. Kang, J. Kodah, Q. Guan, X. Li, W.V. Murray, J. Org. Chem. 70 (2005) 1957–1960.
[44] X.-C. Wang, G.-J. Yang, X.-D. Jia, Z. Zhang, Y.-X. Da, Z.-J. Quan, Tetrahedron 67 (2011) 3267–3272.
[45] P. Biginelli, Gazz. Chim. Ital. 23 (1893) 360–416.
[46] C.O. Kappe, Acc. Chem. Res. 33 (2000) 879–888.
[47] M.A. Kolosov, V.D. Orlov, Mol. Diversity 13 (2009) 5–25.
[48] G.T. Kerr, J. Phy. Chem. 72 (1968) 2594–2596.
[49] R.M. Barrer, M.V. Makki, Can. J. Chem. 42 (1964) 1481–1487.
[50] U. Lohse, E. Loffler, M. Hunger, J. Stockner, V. Patzelovía, Zeolites 7 (1987) 11–13.
[51] P.K. Maher, F.D. Hunter, J. Scherzer, Adv. Chem. Ser. 101 (1971) 266–278.
[52] Q.L. Wang, G. Giannetto, M. Torrealba, G. Perot, C. Kappenstein, M. Guisnet, J. Catal. 130 (1991) 459–470.
[53] N. Salman, C.H. Ruscher, J.-C. Buhl, W. Lutz, H. Toufar, M. Stocker, Microporous Mesoporous Mater. 90 (2006) 339–346.
[54] R.M. Silverstein, F.X. Webster, Spectrometric Identification of Organic Com-pounds, 6th ed., Wiley Publisher, 2007.
[55] E.M. Flanigan, H. Khatami, H.A. Szymanski, Infrared structural studies of zeolite frameworks, Molecular Sieve Zeolites- I, E.M. Flanigen, L.B. Sand, vol. 101 of Advances in Chemistry, chapter 16, American Chemical Society : Washington, DC, 1974, pp. 201–229.
[56] Z. Yan, D. Ma, J. Zhuang, X. Liu, X. Liu, X. Han, X. Bao, F. Chang, L. Xu, Z. Liu, J. Mol. Catal. A: Chem. 194 (2003) 153–167.
[57] C. Covarrubias, R. Quijada, R. Rojas, Appl. Catal. A: Gen. 347 (2008) 223–233.
[58] Z. Qin, B. Shena, Z. Yu, F. Deng, L. Zhao, S. Zhou, D. Yuan, X. Gao, B. Wang, H. Zhao, H. Liu, J. Catal. 298 (2013) 102–111.
[59] G.T. Kerr, J. Phys. Chem. 71 (1967) 4155–4156.
[60] G.T. Kerr, J. Catal. 15 (1969) 200–204.
[61] A.H. Alwash, A.Z. Abdullah, N. Ismail, Adv. Chem. Eng. Sci. 3 (2013) 113–122.
[62] V. Valtchev, G. Majano, S. Mintova, J.P. Ramírez, Chem. Soc. Rev. 42 (2013) 263–290.
[63] E. Senderov, I. Halasz, D.H. Olson, Microporous Mesoporous Mater. 186 (2014) 94–100.
[64] P.j. Grobet, P.A. Jacobs, H.K. Beyer, Zeolites 6 (1986) 47–50.
[65] P. Fejes, I. Hannus, I. Kiricsi, H. Pfeifer, D. Freude, W. Oehme, Zeolites 5 (1985) 45–48.
[66] P.K. Dutta, D.C. Shieh, M. Puri, Zeolites 8 (1988) 306–309.
[67] S. Ntais, A.M. Moschovi, V. Dracopoulos, V. Nikolakis, ECS Trans. 33 (2010) 41–47.
[68] A.R. Hajipour, F. Rafiee, Org. Prep. Proced. Int. 42 (2010) 285–362.
[69] C.H. Rüscher, J.-C. Buhl, W. Lutz, in: A. Galarneau, F. Di Renzo, F. Fajula, J. Vedrine (Eds.), Studies in Surface Science and Catalysis, vol. 135, Elsevier, Amsterdam, 2001, p. 1, 13-P15.